Light hadron spectroscopy on coarse lattices with $O(a^2)$ mean-field-improved actions

Frank X. Lee*

Center for Nuclear Studies, Department of Physics, The George Washington University, Washington, DC 20052;
Jefferson Lab, 12000 Jefferson Avenue, Newport News, Virginia 23606;
Department of Physics, University of Colorado, Boulder, Colorado 80309-0446;
and TRIUMF, 4004 Wesbrook Mall Vancouver, British Columbia, Canada V6T 2A3

Derek B. Leinweber[†]

Department of Physics and Mathematical Physics, University of Adelaide 5005, Adelaide, Australia
and Department of Physics, University of Washington, Seattle, Washington 98195

The masses and dispersions of light hadrons are calculated in lattice QCD using an $O(a^2)$ tadpole-improved gluon action and an $O(a^2)$ tadpole-improved next-nearest-neighbor fermion action originally proposed by Hamber and Wu. Two lattices of constant volume with lattice spacings of approximately 0.40 fm and 0.24 fm are considered. The results reveal some scaling violations at the coarser lattice spacing on the order of 5%. At the finer lattice spacing, the nucleon to rho mass ratio reproduces state-of-the-art results using unimproved actions. Good dispersion and rotational invariance up to momenta of $pa \simeq 1$ are also found. The relative merit of alternative choices for improvement operators is assessed through close comparisons with other plaquette-based tadpole-improved actions. [S0556-2821(99)03807-2]

PACS number(s): 12.38.Gc, 14.20.−c, 14.40.−n

I. INTRODUCTION

Lattice discretization of the continuum QCD action introduces errors at finite lattice spacing a. The standard Wilson gauge action has $O(a^2)$ errors and the standard Wilson fermion action has $O(a)$ errors. Simulations using these actions have shown that lattice spacings of 0.1 fm or less and lattice volumes of 24^4 or larger are needed in order to hold systematic errors to the 10% level. Such simulations are major undertakings and require enormous computing power to extract even the most basic of hadronic observables, the hadron masses (see [1] for an example and [2] for a recent review).

During the past few years, considerable efforts have been devoted to improving lattice actions. The idea is to reduce or remove the discretization errors from the actions so that they have better continuum-like behavior. At the same time, errors due to the lattice regularization are accounted for through the renormalization of the coefficients multiplying the improvement operators. The hope is the use of improved actions will allow one to simulate efficiently and accurately on coarse lattices, such that computer resources may be redirected to the simulation of QCD rather than quenched QCD. Moreover, one may turn the focus of investigation towards quantities of experimental interest.

The way to develop improved discretizations of continuum actions is not unique. There are numerous programs in this endeavor having their foundation in one of two formulations. One is based on lattice perturbation theory which is used to derive the renormalized coefficients through a mean-field reordering of the perturbative expansion, as recently reviewed by Lepage [3]. The other is based on renormalization group theory to construct fixed-point (or perfect) actions, as recently reviewed by Hasenfratz [4].

In the pure gauge sector, the $O(a^2)$ tadpole-improved action of [5] leads to dramatic improvement in the static potential and glueball masses [6] up to lattice spacings of 0.4 fm. Excellent scaling and topological properties have been demonstrated in fixed-point actions [7]. In the light quark sector, hadron spectroscopy has been investigated with a variety of improved actions including the $O(a)$-improved Sheikoleslami-Wohlert (SW) action [8], the $O(a^2)$-improved D234 action [9] and its variants [3,10], and the Dχ34 action of Hamber and Wu [11–14] considered here. Fixed-point fermion actions have been studied in free field theory [15,16] and in simulations [17].

In the present work, we report further calculations of the light hadron spectrum using the $O(a^2)$ tadpole-improved gluon action of [5] and the Dχ34 action proposed by Hamber and Wu [11] many years ago. This action is an $O(a^2)$ next-nearest-neighbor fermion action with tadpole-improved estimates of the coupling renormalizations. This action is selected primarily due to its simplicity. The cost of simulating it is about a factor of two as compared to standard Wilson fermions. Our goal is to study its feasibility as an alternative action to SW which has the clover term, or to D234, which has both next-nearest-neighbor couplings and the clover term.

This work extends previous studies of the Dχ34 action [13,14] through finer lattice spacings, improved statistics, and the simulation of additional observables. In particular, we examine dispersion relations and test the rotational symmetry of both the gauge and the fermion actions. Hadron mass ratios are calculated for a wide variety of hadrons including hyperons. To explore scaling violations, we consider two coarse lattices of approximately fixed physical volume:

*Email address: fxlee@gwu.edu

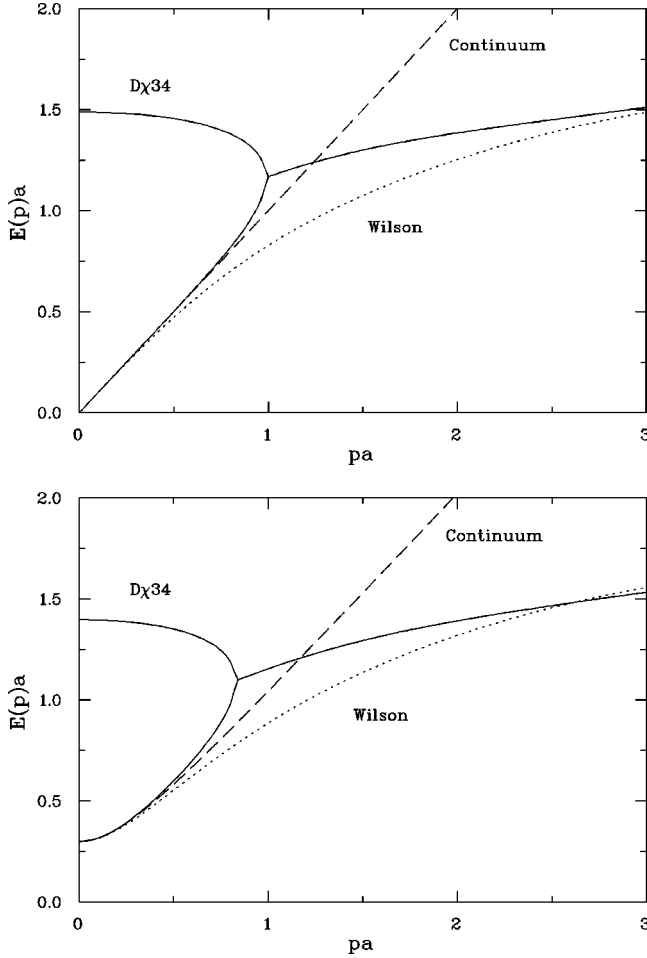[†]Email address: dleinweb@physics.adelaide.edu.au

FIG. 1. Free dispersion relations for $D\chi34$, Wilson, and continuum fermions. Momentum p is along the $(1,1,0)$ direction. Beyond the $D\chi34$ branch point, the real part of the two conjugate roots is shown. The upper graph is for bare mass $ma=0$, the lower $ma=0.3$.

$6^3\times12$ at a lattice spacing of 0.40 fm and $10^3\times16$ at 0.24 fm.

II. IMPROVED LATTICE ACTIONS

A. Gauge action

The improved gauge action employed in this investigation is given by [5]

$$S_G = \beta \sum_{\text{pl}} \frac{1}{3}\text{Re Tr}(1-U_{\text{pl}}) - \frac{\beta}{20u_0^2}\sum_{\text{rt}}\frac{1}{3}\text{Re Tr}(1-U_{\text{rt}}). \quad (1)$$

The second term removes the $O(a^2)$ errors at tree level. Perturbative corrections are estimated to be of the order of 2–3 % [5]. Here, U_{rt} denotes rectangular 1×2 plaquettes. u_0 is the tadpole factor that largely corrects for the large quantum renormalization of the links $U_\mu(x) = \exp[ig\int_x^{x+a\hat\mu}A(y)\cdot dy]$. In this calculation we use the mean plaquette to estimate u_0,
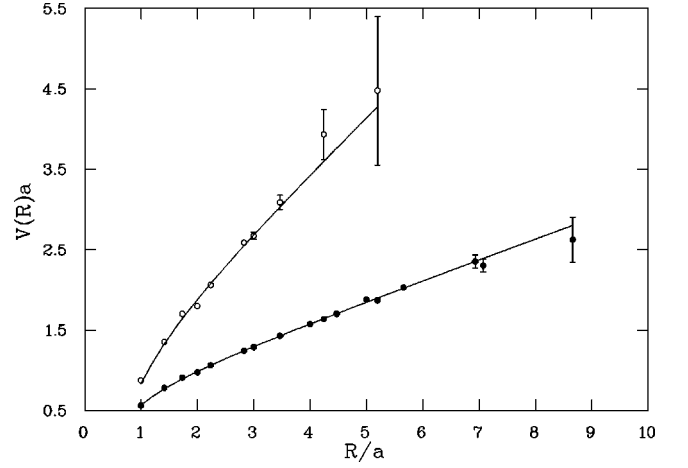

FIG. 2. Static potential from Wilson loops. The open circles are for $\beta=6.25$, the solid circles for $\beta=7.0$. The lines are best fits. The statistical errors were from 200 configurations in both cases.

$$u_0 \equiv \left(\frac{1}{3}\text{Re Tr}\langle U_{\text{pl}}\rangle\right)^{1/4}, \quad (2)$$

and will focus our evaluation of lattice action improvement on other plaquette-based improved actions. u_0 is determined self-consistently in the simulation. An alternative choice is to use the mean link in Landau gauge $u_0\equiv\langle\frac{1}{3}\text{Tr }U_\mu\rangle_{\text{LG}}$ [10].

B. Dχ34 fermion action

The improvement program of Sheikoleslami and Wohlert [18] provides a systematic approach to the improvement of lattice fermion actions. However, the on-shell improvement program leaves some freedom in the relative values of the coefficients of the improvement operators. In this investigation, we consider a specific case of the general class of D234 actions [10] in which the improvement parameters are tuned to remove the second-order chiral-symmetry-breaking Wilson term. This fermion action may be written

$$M_{\text{D}\chi34} = m_q + \gamma\cdot\nabla + \frac{1}{6}\sum_\mu\left(-a^2\nabla_\mu\Delta_\mu + ba^3\Delta_\mu^2\right) \quad (3)$$

where

$$\nabla_\mu\psi(x) = \frac{1}{2a}[U_\mu(x)\psi(x+\mu) - U_\mu^\dagger(x-\mu)\psi(x-\mu)] \quad (4)$$

and

TABLE I. String tension and R_0 extracted from the static potential.

β	σa^2	R_0/a	R_{min}/a	R_{max}/a	χ^2/N_{DF}
6.25	0.81(23)	1.26(11)	1.00	4.24	1.46
7.00	0.254(8)	2.279(18)	1.73	6.93	0.91

TABLE II. Summary of lattice parameters for the spectrum calculations. N_U is the number of configurations considered. The second kappa was selected as the one that corresponds to the strange quark mass.

Lattice	β	N_U	u_0	κ	κ_{cr}
$6^3 \times 12$	6.25	155	0.820	0.175, 0.177, 0.180, 0.183, 0.187	0.1967(2)
$10^3 \times 16$	7.00	100	0.866	0.170, 0.172, 0.174, 0.176, 0.178	0.1823(3)

$$\Delta_\mu \psi(x) = \frac{1}{a^2} [U_\mu(x) \psi(x+\mu) + U_\mu^\dagger(x-\mu) \psi(x-\mu)$$

$$- 2\psi(x)]. \tag{5}$$

The second-order term of the D234 action

$$\sum_\mu \Delta_\mu + \frac{1}{2} \sigma \cdot F \tag{6}$$

breaks chiral symmetry and does not appear in the $D\chi 34$ action. However, the fourth-order term of Eq. (3) also breaks chiral symmetry and provides for the removal of the fermion doublers.

Explicit evaluation of Eq. (3) combined with a Wilson-fermion-style field renormalization factor of $(3\kappa/2)$ discloses the following simple fermion action [11,12]:

$$S_F = \sum_x \bar{\psi}(x) \psi(x) - \kappa \sum_{x,\mu} \left[\bar{\psi}(x)(b - \gamma_\mu) \frac{U_\mu(x)}{u_0} \psi(x+\mu) \right.$$

$$+ \bar{\psi}(x+\mu)(b + \gamma_\mu) \frac{U_\mu^\dagger(x)}{u_0} \psi(x) + \bar{\psi}(x) \left(-\frac{1}{4} b + \frac{1}{8} \gamma_\mu \right)$$

$$\times \frac{U_\mu(x)}{u_0} \frac{U_\mu(x+\mu)}{u_0} \psi(x+2\mu) + \bar{\psi}(x+2\mu)$$

$$\times \left(-\frac{1}{4} b - \frac{1}{8} \gamma_\mu \right) \frac{U_\mu^\dagger(x+\mu)}{u_0} \frac{U_\mu^\dagger(x)}{u_0} \psi(x) \right]. \tag{7}$$

The tadpole-improvement factors are explicit here. These coefficients remove both $O(a)$ and $O(a^2)$ errors at the tree level. The bare quark mass is related to κ and b through

$$m_q = \frac{2}{3\kappa} - 4b. \tag{8}$$

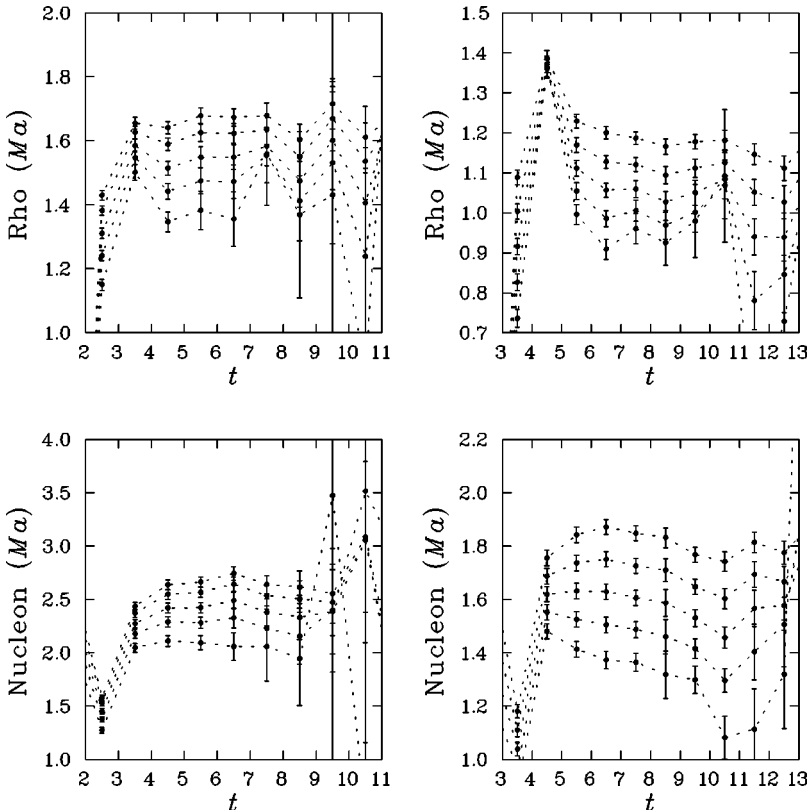Thus the renormalized quark mass is given by

FIG. 3. Effective mass plots for the ρ and nucleon. The first column illustrates results for the coarse lattice while the second is for the finer lattice. Propagator sources are at $t=2$ and 3 for the coarse and fine lattices respectively. The five quark masses decrease by value from top down.
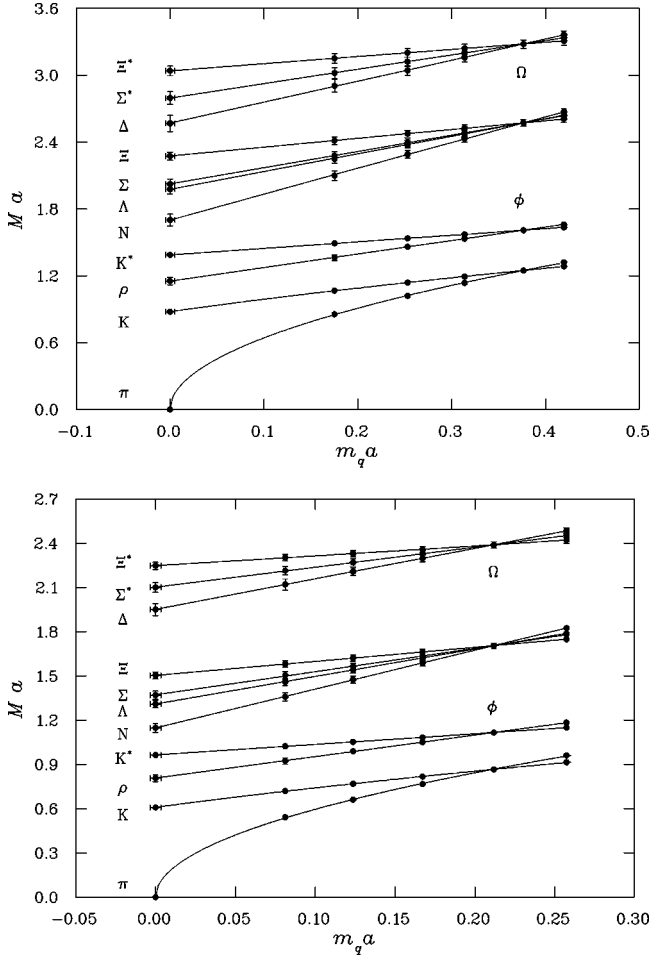
FIG. 4. Hadron masses in lattice units as a function of m_q. The upper graph is for the coarser lattice, the lower for the finer lattice. The lines are chiral fits as discussed in the text. For better viewing, the decuplet masses are shifted upward by 1/2 unit.

$$m_q = \frac{2}{3}\left(\frac{1}{\kappa} - \frac{1}{\kappa_{cr}}\right). \qquad (9)$$

The wave function renormalization factor is also modified:

$$\psi_{cont} = \sqrt{\frac{3\kappa}{2}}\,\psi_{latt}. \qquad (10)$$

The standard Wilson action can be recovered by truncating the two-link terms of the action, redefining κ and renormalizing the fermion field operators.

Free dispersion relations can be obtained by locating the poles in the fermion propagator. Figure 1 shows free dispersion relations for the continuum, Wilson, and Dχ34 fermions. It is clear that Dχ34 fermions follow the continuum more closely than Wilson fermions. Note that there exists an unphysical high energy doubler (or ghost) in the Dχ34 action. It is very similar to that for the D234 action [9] and is a general feature of fermions with next-nearest-neighbor couplings. The doubler can be ''pushed away'' from the low momentum region by various techniques, such as tuning the

value of b or using an anisotropic lattice [10]. We simulate with $b=1$, which gives good dispersion to $pa \sim 1$ as illustrated in Fig. 1.

III. LATTICE SIMULATIONS

A. Methods and parameters

Quenched gauge configurations were generated using the Cabibbo-Marinari pseudo-heat-bath method [20]. Periodic boundary conditions were used in all directions for the gauge field and in spatial directions for the fermion field. Dirichlet boundary conditions were used for the fermion field in the time direction. Configurations separated by 300 sweeps were selected after 4000 thermalization sweeps from a cold start.

Wilson loops were computed using a method developed in Ref. [21]. Both on-axis and off-axis loops were considered. The static potential was determined by fitting $\exp[-V(R)T] = W(R,T)$. The string tension σ was extracted from the ansatz $V(R) = V_0 + \sigma R - E/R$ where V_0 and E are constants. Figure 2 shows our results. Good rotational invariance of the static potential is observed. Table I gives the extracted string tension and the R_0 parameter, defined by $R^2 dV(R)/dR = 1.65$ at R_0 [22]. Its physical value is $R_0 \simeq 0.50$ fm and it is independent of the quenched approximation. Using the string tension $\sqrt{\sigma} = 465$ MeV from a recent study [23] to set the scale, the lattice spacings were determined as 0.38(6) fm and 0.22(1) fm, respectively. Using R_0 to set the scale, they are 0.40(3) fm and 0.22(1) fm. R_0 depends less on the functional form of $V(R)$ than the string tension.

Five quark propagators were computed by the stabilized biconjugate gradient algorithm [24] for each configuration. The five κ values correspond to quark masses of roughly 210, 180, 150, 120, 90 MeV, respectively, for both lattices. The second value, 180 MeV, was taken as the strange quark mass. A point source was used at space-time location $(x,y,z,t) = (1,1,1,2)$ on the $6^3 \times 12$ lattice and $(1,1,1,3)$ on the $10^3 \times 16$ lattice with the origin at $(x,y,z,t) = (1,1,1,1)$. We observed no exceptional configurations in all cases. The gauge-invariant smearing method of [25] was applied at the sink to increase the overlap of the interpolating operators with the ground states. Table II shows a summary of the parameters.

Statistical errors were estimated in a third-order, single-elimination jackknife, with bias corrections [26]. A third-order jackknife provides uncertainty estimates for the correlation functions, fits to the correlation functions, and quantities extrapolated to the chiral limit.

B. Effective masses

Masses were extracted from lattice correlation functions in several time slice intervals. The effective hadron mass as a function of time is defined by

$$M(t+1/2) = \log[G(t)] - \log[G(t+1)] \qquad (11)$$

where $G(t)$ is the standard two-point function in Euclidean space-time. As usual, effective mass plots for the pion are

TABLE III. Hadron masses as a function of m_q (both in lattice units). The results were extracted from time slices 4–8 on the coarser lattice and 6–9 on the finer lattice. The last column reports results after extrapolations to the chiral limit.

$6^3 \times 12$ lattice at $\beta = 6.25$

Hadron	$m_q = 0.42$	$m_q = 0.37$	$m_q = 0.31$	$m_q = 0.25$	$m_q = 0.17$	$m_q = 0$
π	1.321(6)	1.248(6)	1.136(6)	1.020(7)	0.855(8)	0
K	1.29(1)	1.25(1)	1.19(1)	1.14(1)	1.07(1)	0.88(1)
ρ	1.66(1)	1.61(1)	1.53(2)	1.46(2)	1.36(3)	1.15(4)
K^*	1.64(1)	1.61(1)	1.57(2)	1.54(2)	1.49(2)	1.39(2)
N	2.67(3)	2.57(3)	2.43(3)	2.29(4)	2.10(5)	1.70(6)
Λ	2.64(3)	2.57(3)	2.48(3)	2.38(3)	2.25(4)	1.98(5)
Σ	2.64(3)	2.57(3)	2.48(3)	2.39(3)	2.28(4)	2.02(5)
Ξ	2.61(3)	2.57(3)	2.52(3)	2.48(3)	2.41(3)	2.27(4)
Δ	2.86(4)	2.78(4)	2.66(4)	2.54(4)	2.40(6)	2.07(7)
Σ^*	2.83(4)	2.78(4)	2.70(4)	2.62(4)	2.52(5)	2.30(6)
Ξ^*	2.82(4)	2.78(4)	2.74(4)	2.70(4)	2.65(4)	2.54(5)

$10^3 \times 16$ lattice at $\beta = 7.0$

Hadron	$m_q = 0.26$	$m_q = 0.21$	$m_q = 0.17$	$m_q = 0.13$	$m_q = 0.08$	$m_q = 0$
π	0.967(7)	0.871(7)	0.772(7)	0.667(7)	0.548(8)	0
K	0.920(7)	0.871(7)	0.823(7)	0.775(7)	0.726(7)	0.608(5)
ρ	1.19(1)	1.12(1)	1.05(1)	0.99(2)	0.92(2)	0.80(2)
K^*	1.15(1)	1.12(1)	1.08(1)	1.05(1)	1.02(2)	0.96(2)
N	1.86(2)	1.74(2)	1.62(2)	1.50(2)	1.37(3)	1.15(3)
Λ	1.82(2)	1.74(2)	1.65(2)	1.57(2)	1.48(2)	1.33(2)
Σ	1.81(1)	1.74(2)	1.66(2)	1.59(2)	1.52(2)	1.38(3)
Ξ	1.78(2)	1.74(2)	1.69(2)	1.65(2)	1.61(2)	1.53(2)
Δ	2.00(2)	1.90(2)	1.80(2)	1.71(3)	1.62(4)	1.44(4)
Σ^*	1.97(2)	1.90(2)	1.84(2)	1.78(3)	1.72(3)	1.60(3)
Ξ^*	1.94(2)	1.90(2)	1.87(2)	1.84(2)	1.81(3)	1.75(3)

very flat. All fits of time slices 4–10 on our coarse lattice and 6–12 on our fine lattice agree within one standard deviation.

Figure 3 displays effective mass plots for the ρ meson and nucleon. The effective masses show an irregular behavior at the first two time slices away from the point source. This is the practical manifestation of the massive algorithmic ghosts depicted in the upper branches of Fig. 1. As long as these ghost poles in the quark propagator are at sufficiently high energies, their effects disappear at larger times. While the presence of these ghost poles prevent the use of the first couple of time slices, there is otherwise no problem with the transfer matrix [27].

We also note that the effective nucleon mass rises from below as a function of Euclidean time. This behavior reflects the use of smeared sink propagators. Excited states having nodal wave functions can reduce the correlation function when smeared sources or sinks are used. This suppression in the correlation function leads to a suppression of the effective mass at early Euclidean times. As such, the effective mass will be somewhat small until these excited states are exponentially suppressed by Euclidean-time evolution. These results indicate that improved smearing functions will incorporate more localized smearing extents.

The ρ meson displays good plateau behavior. We find $\chi^2/N_{DF} \sim 0.5$ for correlation function fits from $t = 4$ to 10 on

our coarse lattice and $\chi^2/N_{DF} \simeq 0.7$ for correlation function fits from $t = 6$ to 11 on our fine lattice. Again, all fits agree within one standard deviation.

On our coarse lattice the nucleon mass displays good plateau behavior. The χ^2/N_{DF} ranges from 1.0 to 0.1 for the lightest quark mass. All fits in the interval 4 to 10 agree within one standard deviation.

On our fine lattice, plateau behavior for the nucleon mass is excellent within the regime $t = 6$–9. For the heaviest three quark masses, however, the χ^2/N_{DF} identifies two separate fitting regimes providing acceptable fits, namely 6–9 and 9–12. The latter regime disappears for the lightest two quark masses while the former regime grows, providing acceptable fits for $t = 6$–10. Since the effective masses rise from below as a function of t for smeared sinks, we report results for the regime $t = 6$–9 where the signal is less likely to be dominated by noise.

We note that this drift in the effective mass plot is only significant as measured by the χ^2/N_{DF} for the ground state nucleon mass. We find that other quantities such as the nucleon energy or ρ-meson mass are sufficiently correlated to provide results insensitive to the fit regime. For example, dispersion relations agree within one standard deviation for all fits of $t = 6$–12 with no systematic drift in the central

TABLE IV. Mass ratios after extrapolation to the chiral limit. a_ρ and a_N are lattice spacings set by the rho mass (770 MeV) and the nucleon mass (938 MeV).

	$\beta=6.25$	$\beta=7.0$	Expt.
a_{st}	0.40(3) fm	0.220(2) fm	
a_ρ	0.30(1) fm	0.205(6) fm	
a_N	0.36(1) fm	0.242(6) fm	
Vector/vector			
K^*/ρ	1.20(2)	1.20(2)	1.16
ϕ/ρ	1.40(3)	1.39(3)	1.32
Octet/octet Λ/N	1.16(2)	1.16(1)	1.19
Σ/N	1.19(2)	1.20(1)	1.27
Ξ/N	1.34(3)	1.33(2)	1.40
Decuplet/decuplet Σ^*/Δ	1.12(1)	1.11(1)	1.12
Ξ^*/Δ	1.24(3)	1.22(2)	1.24
Ω/Δ	1.34(3)	1.33(2)	1.36
Pseudoscalar/vector			
K/ρ	0.76(2)	0.75(2)	0.64
Octet/vector			
N/ρ	1.48(6)	1.44(5)	1.22
Λ/ρ	1.72(6)	1.66(5)	1.45
Σ/ρ	1.76(6)	1.72(5)	1.55
Ξ/ρ	1.97(6)	1.91(6)	1.71
Decuplet/vector Δ/ρ	1.79(7)	1.77(5)	1.60
Σ^*/ρ	2.00(6)	1.97(6)	1.80
Ξ^*/ρ	2.20(7)	2.16(6)	1.99
Ω/ρ	2.40(7)	2.35(6)	2.17
Decuplet/Octet Δ/N	1.21(5)	1.23(2)	1.31
Σ^*/N	1.35(5)	1.37(2)	1.47
Ξ^*/N	1.49(4)	1.50(3)	1.63
Ω/N	1.63(4)	1.64(3)	1.78

values. Moreover, the extrapolated nucleon to rho mass ratios for the time slice regimes 6–9 and 9–12 are 1.44(5) and 1.41(13) respectively. Again, the deviation of central values of the distributions is small relative to the statistical uncertainties.

Effective mass plots for Δ are acceptably flat but suffer a loss of signal earlier in Euclidean time as expected. On our coarse lattice we find acceptable $\chi^2/N_{DF}\simeq1.0\rightarrow0.4$ for intervals $t=4$ or 5–10 with smaller values corresponding to lighter masses. On our fine lattice we find acceptable $\chi^2/N_{DF}\simeq1.0\rightarrow0.6$ for intervals $t=6$ or 7–12, again with smaller values corresponding to lighter masses.

In summary, we report values taken from covariance matrix fits to the time slice interval 4–8 on our coarse lattice

and 6–9 on our fine lattice. These regimes provide the best signal-to-noise and good correlated χ^2/N_{DF}.

C. Hadron masses

Figure 4 shows the extracted hadron masses plotted as a function of the quark mass. For future reference, these results are tabulated in Table III. κ_{cr} is determined by linearly extrapolating m_π^2 as a function of m_q to zero. Similarly, the pseudoscalar kaon is extrapolated via $m_K^2=c_0+c_1m_q$. The form $M=c_0+c_1m_q$ is used for all other extrapolations to the chiral limit. Fits including an additional term $c_2m_q^{3/2}$ are also considered and similar results are found with slightly larger error bars. The correct ordering of all the states is clearly seen at both values of β.
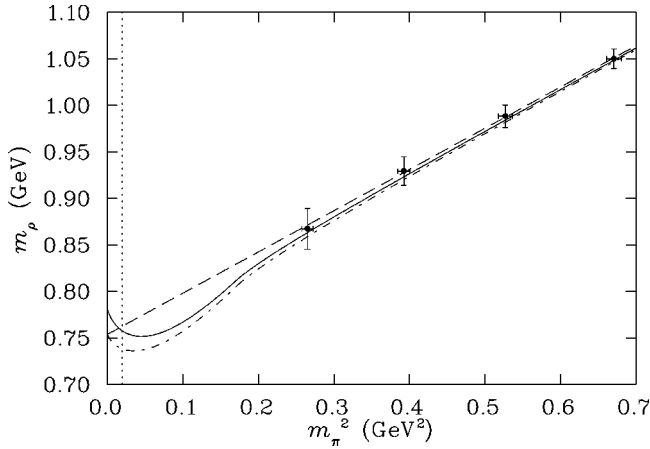
FIG. 5. Plot of the ρ-meson mass as a function of the squared pion mass obtained from our finer lattice. a_ρ has been used to set the scale. The dashed line illustrates the standard linear extrapolations of m_π^2 and m_ρ. The solid and dot-dashed curves include the two-pion self-energy of the ρ meson [30] for dipole dispersion cutoff values of 1 and 2 GeV respectively. The increase in the slope at $m_\rho/m_\pi = 1.8$ ($m_\pi^2 \simeq 0.21$) provided by the two-pion self-energy is the right order of magnitude to restore agreement with the empirical value.

Ratios of the chirally extrapolated masses are given in Table IV along with the ratios as observed in nature [28]. At $\beta = 7.0$ the lattice spacing estimates follow the familiar pattern having the value based on the string tension lying between that of the ρ and nucleon based values. This is most likely an artifact of the quenched approximation. However, at $\beta = 6.25$ we find significant disagreement among the values and an unusual reordering of values.

Focusing first on ratios of hadrons having the same angular momentum, we see very little change in the values as the lattice spacing is decreased. These ratios are also remarkably similar to those observed in nature, despite the fact that these are quenched QCD calculations. In addition, these ratios support our selection for the strange quark mass.

This close resemblance to nature is not shared by ratios of hadrons with different angular momentum. All four classes of ratios significantly disagree with those of nature. Once again we see the familiar quenched artifact of the octet/vector ratio being too large and the decuplet/octet ratio being too small.

The standard failure of the K/ρ mass ratio in the quenched approximation is also seen here. This shortcoming has been widely realized through an examination of the J-parameter [29] defined by

$$J = m_\rho \frac{dm_\rho}{dm_\pi^2}\bigg|_{m_\rho/m_\pi = 1.8} \simeq m_{K*} \frac{m_{K*} - m_\rho}{m_K^2 - m_\pi^2}. \quad (12)$$

Empirically this ratio is 0.48. However, we find 0.40 on our coarse lattice and 0.38 on our fine lattice. The physics associated with this discrepancy was first reported in Ref. [30]. There it was pointed out that the self-energy generated by two-pion intermediate states of the ρ-meson, which is ex-

cluded in the quenched approximation, acts to increase the J parameter. Figure 5 provides a sketch of how including the two-pion self-energy of the ρ can increase the value of J from 0.38 to 0.46.

Perhaps the most important information displayed in Table IV is that the octet/vector mass ratios display less than satisfactory scaling for the larger lattice spacing. To further examine scaling and make contact with other studies, we focus on the N/ρ mass ratio which is among the most revealing of ratios.

Figure 6 shows a comparison of the N/ρ mass ratio versus $M_\rho a$ at the chiral limit. Figure 7 shows the N/ρ mass ratio as a function of $M_\rho a$ at a fixed π/ρ mass ratio of 0.7 [32]. This method is free of complications from chiral extrapolations. Both cases clearly show the improvement provided by the
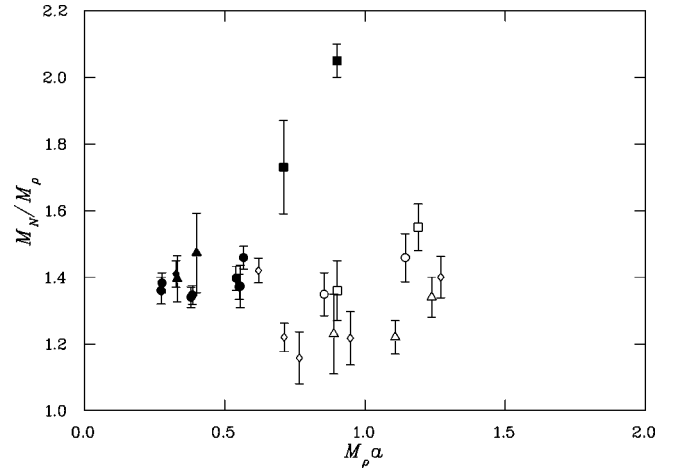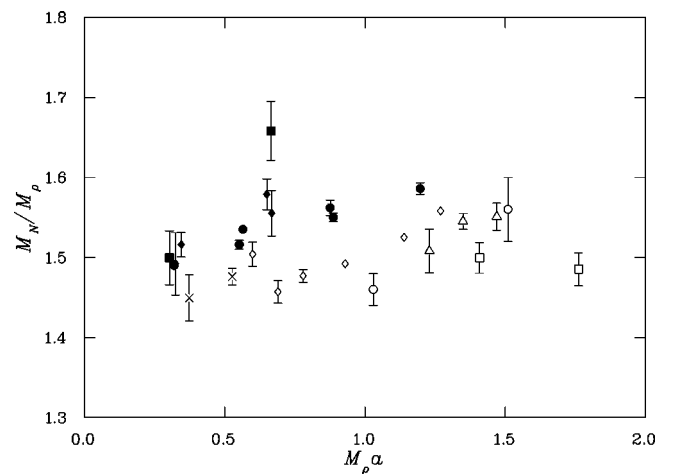

FIG. 6. The N/ρ mass ratio versus $M_\rho a$ at the chiral limit. Solid symbols denote the standard Wilson action. Open symbols denote improved actions including SW ($\diamond$)[8], D234 9 ($\triangle$)[9], Dχ34 ($\square$)[13], and Dχ34 ($\bigcirc$) (this work).

FIG. 7. The N/ρ mass ratio versus $M_\rho a$ at a fixed π/ρ mass ratio of 0.7 for various actions. The solid symbols denote the standard actions: Wilson (square and diamond), staggered (circle). The open symbols denote improved actions: nonperturbatively-improved SW ($\times$)[31], fixed-point action ($\square$)[17], SW ($\diamond$), D234 ($\triangle$), and Dχ34 ($\bigcirc$) (this work).

TABLE V. Standard Wilson action results from CP-PACS at $\beta=5.9$ on a $32^3 \times 56$ lattice are compared with Dχ34 action results on our fine $10^3 \times 16$ lattice after linear extrapolation to the chiral limit.

	Wilson	Dχ34
Vector/vector		
K^*/ρ	1.16	1.20(2)
ϕ/ρ	1.32	1.39(3)
Octet/vector		
N/ρ	1.39	1.44(5)
Decuplet/vector		
Δ/ρ	1.78	1.77(5)
Σ^*/ρ	1.93	1.97(6)
Ξ^*/ρ	2.07	2.16(6)
Decuplet/decuplet		
Σ^*/Δ	1.08	1.11(1)
Ξ^*/Δ	1.16	1.22(2)

Dχ34 action. Indeed, the Dχ34 action has reproduced the state-of-the-art quenched QCD nucleon to rho mass ratio using unimproved actions at coarse lattice spacings of 0.24 fm. Our results at the chiral limit are compatible with those in [13], but lie slightly above the SW and D234 results. The results from various improved actions at fixed π/ρ ratio show a certain degree of universality over a wide range of lattice spacings. The performance of fixed-point actions at very coarse lattice spacings is remarkable.

To further explore the level of improvement afforded by the Dχ34 action we compare our results with standard Wilson action results from the CP-PACS Collaboration [2]. Table V compares the CP-PACS results at $\beta=5.9$ on a $32^3 \times 56$ lattice with our results. We include results where sufficient data are available to allow a comparison utilizing the same extrapolation procedure. To match the strange quark masses as closely as possible, we select the CP-PACS results which utilize the ϕ-meson mass to set the strange-quark mass. Our results lie above the CP-PACS results for strange hadrons suggesting a mismatch in the strange quark mass. The discrepancy is proportional to the number of strange quarks in the hadron and promises improved agreement if our strange-quark mass is reduced. Agreement is seen for the non-strange hadron-mass ratios.

D. Dispersion and rotational symmetry

In addition to mass ratios, hadron states at finite momentum projections $\vec{p}a=\vec{n}(2\pi/L)$ were also calculated. Dispersion was examined by calculating the effective speed of light, c_{eff}, defined by $c_{eff}^2=[E^2(p)-E^2(0)]/p^2$, which is to be compared with 1.

A comparison with SW and D234 lattice actions [9] is made in Table VI. The lattice spacings are based on charmonium for SW and D234 actions whereas the static quark po-

TABLE VI. Comparison of SW, D234 and Dχ34 actions for the speed of light squared obtained from the dispersion of π and ρ mesons at $m_\pi/m_\rho \simeq 0.7$ for $pa=(2\pi/L)$.

Hadron	a (fm)	SW	D234	Dχ34
π	0.40	0.63(2)	0.95(2)	0.99(3)
π	0.24		0.99(4)	1.04(4)
ρ	0.40	0.48(4)	0.93(3)	0.93(6)
ρ	0.24		1.00(6)	0.99(6)

tential is used for our results. As such, the lattice spacings in Table VI are approximate. Lattice volumes range from 2.0 to 2.4 fm. Dχ34 results are based on simulations at $\kappa=0.183$ for our coarse lattice and $\kappa=0.176$ on our fine lattice. The dispersion for the $O(a)$-improved SW action is very poor relative to the excellent dispersions of the next-nearest-neighbor improved Dχ34 actions. The Dχ34 dispersion is excellent even at our coarse lattice spacing.

Rotational symmetry is explored in Table VII, which reports results for $m_q \sim 180$ MeV. At the coarser lattice spacing, some drift in the central values is seen for the pion and nucleon. The drift in the pion is similar to that seen for the D234c action reported in Ref. [3]. However, the drift in dispersion for the ϕ meson reported in Ref. [3] is not apparent in our results for the Dχ34 action. However, a similar drift may be hidden in the uncertainties. The Dχ34 action has much better rotational symmetry than the SW action [3]. Moreover, the Dχ34 action provides satisfactory dispersion at our finer lattice spacing and is competitive with the D234 action [9].

IV. CONCLUSIONS

We have computed masses and dispersion relations of light hadrons in lattice QCD using tree-level $O(a^2)$ tadpole-improved gauge and fermion actions. Compared to standard Wilson actions, the gluon action has an additional six-link (rectangle) term while the Dχ34 fermion action has an additional two-link (next-nearest-neighbor) term. These actions have the appeal of being simple to implement and inexpensive to simulate.

The cost of a quenched lattice simulation scales like the inverse lattice spacing to the sixth power [19]. Considering this fact alone, the savings from our fine $10^3 \times 16$ lattice at

TABLE VII. Evaluation of dispersion and rotational invariance via the effective speed of light. The results are for $m_q \sim 180$ MeV.

a (fm)	$\vec{n}$	π	ϕ	N	Ω
0.40	(1,0,0)	0.98(2)	0.91(4)	1.00(7)	0.99(12)
	(1,1,0)	0.91(4)	0.91(6)	0.94(8)	0.91(7)
	(1,1,1)	0.86(9)	0.92(10)	0.92(7)	0.90(10)
0.24	(1,0,0)	1.04(3)	1.02(4)	1.10(6)	1.06(7)
	(1,1,0)	1.05(4)	1.02(4)	1.06(5)	1.11(5)
	(1,1,1)	0.98(6)	0.98(6)	1.06(6)	1.06(5)

$a = 0.24$ relative to a $32^3 \times 48$ lattice at $a = 0.1$ fm for standard Wilson gauge and fermion actions is a factor of approximately 200. Allowing a factor of 2 and 3 for the cost of the improved fermion and gauge actions used here leaves a net improvement factor approaching two orders of magnitude. The ultimate performance enhancement offered by improved-action algorithms also requires a careful analysis of statistical fluctuations, and this is currently under investigation [33].

A great deal of effort is being directed toward finding the ultimate improved action that will facilitate simulations on the coarsest of lattices. We note, however, that many quantities of phenomenological interest such as hadron form factors involve momenta on the order of a GeV. As such, a highly improved action which is costly to simulate may not be the ideal action for hadron phenomenology, especially for exploratory purposes. Moreover, instanton considerations suggest that lattice spacings the order of 0.2 fm or less are required in order to capture the relevant topological aspects of QCD. At these lattice spacings the efficiency of the $D\chi34$ action becomes even more desirable.

The improvement seen in the mass spectrum is just one aspect of an improved hadronic state on the lattice. We expect similar improvement for matrix element calculations which explore other aspects of the improved hadronic state on the lattice. Of course, form factors will require sufficiently fine lattice spacings such that the desired momentum transfer may be accommodated. The improved dispersion relations demonstrated for this simple next-nearest-neighbor action will allow one to access the momentum transfers of current experimental interest with lattice spacings two to three times larger than that for standard Wilson actions.

The nucleon to rho mass ratio obtained from the $D\chi34$ action at 0.24 fm on a modest $10^3 \times 16$ lattice reproduces the state-of-the-art result using conventional unimproved actions. Excellent dispersion and rotational invariance up to $pa \approx 1$ are also found. These results demonstrate that the $D\chi34$ action can serve as a viable candidate for the study of hadron phenomenology, and in our view is preferable to the highly improved but more costly D234 action. We plan to use the $D\chi34$ action to study hadron properties beyond the spectrum, such as multipole form factors of hadrons in general. These results also bode well for future explorations beyond the quenched approximation.

[1] F. Butler *et al.*, Nucl. Phys. **B430**, 179 (1994).

[2] T. Yoshié, Nucl. Phys. B (Proc. Suppl.) **63**, 3 (1998), in Lattice '98, Proceedings of the International Symposium on Lattice Field Theory, Boulder, CO, 1998, edited by T. DeGrand.

[3] P. Lepage, Nucl. Phys. B (Proc. Suppl.) **60A**, 267 (1998).

[4] P. Hasenfratz, Nucl. Phys. B (Proc. Suppl.) **63**, 53 (1998).

[5] M. Alford, W. Dimm, and P. Lepage, Phys. Lett. B **361**, 87 (1995).

[6] C. Morningstar and M. Peardon, Phys. Rev. D **56**, 4043 (1997).

[7] T. DeGrand *et al.*, Nucl. Phys. **B478**, 349 (1996); **B475**, 321 (1996); **B454**, 615 (1995); **B454**, 587 (1995).

[8] S. Collins, R.G. Edwards, U.M. Heller, and J. Sloan, Nucl. Phys. B (Proc. Suppl.) **47**, 366 (1997); **53**, 206 (1997); **53**, 877 (1997).

[9] M. Alford, T. Klassen, and P. Lepage, Nucl. Phys. B (Proc. Suppl.) **47**, 370 (1996).

[10] M. Alford, T. Klassen, and P. Lepage, Nucl. Phys. B (Proc. Suppl.) **53**, 861 (1997); Nucl. Phys. **B496**, 377 (1997); Nucl. Phys. B (Proc. Suppl.) **63**, 862 (1998).

[11] H. Hamber and C.M. Wu, Phys. Lett. **133B**, 351 (1983); **136B**, 255 (1984).

[12] T. Eguchi and N. Kawamoto, Nucl. Phys. **B237**, 609 (1984).

[13] H.R. Fiebig and R.M. Woloshyn, Phys. Lett. B **385**, 273 (1996).

[14] F.X. Lee and D.B. Leinweber, *Proceedings of 14th International Conference on Particles and Nuclei (PANIC '96)* (World Scientific, Singapore, 1997), p. 617.

[15] W. Bietenholz, R. Brower, S. Chandrasekharan, and U.J. Wiese, Nucl. Phys. B (Proc. Suppl.) **53**, 921 (1997).

[16] T. DeGrand, A. Hasenfratz, P. Hasenfratz, P. Kunszt, and F. Niedermayer, Nucl. Phys. B (Proc. Suppl.) **53**, 942 (1997).

[17] T. DeGrand, Nucl. Phys. B (Proc. Suppl.) **63**, 913 (1998).

[18] B. Sheikoleslami and R. Wohlert, Nucl. Phys. **B259**, 609 (1985).

[19] P. Lepage, Nucl. Phys. B (Proc. Suppl.) **47**, 3 (1996).

[20] N. Cabibbo and E. Marinari, Phys. Lett. **119B**, 387 (1982).

[21] U. Heller, K. Bitar, R. Edwards, and A. Kennedy, Phys. Lett. B **335**, 71 (1994).

[22] R. Sommer, Nucl. Phys. **B411**, 839 (1994).

[23] R. Edwards, U. Heller, and T. Klassen, Nucl. Phys. **B517**, 377 (1998).

[24] A. Frommer, V. Hannemann, B. Nöckel, T. Lippert, and K. Schilling, Int. J. Mod. Phys. C **5**, 1073 (1994).

[25] S. Güsken, Nucl. Phys. B (Proc. Suppl.) **17**, 361 (1990).

[26] B. Efron, SIAM (Soc. Ind. Appl. Math.) Rev. **21**, 460 (1979);

S. Gottlieb, P.B. MacKenzie, H.B. Thacker, and D. Weingarten, Nucl. Phys. **B263**, 704 (1986).

[27] P. Lepage (private communication).

[28] Particle Data Group, L. Montanet *et al.*, Phys. Rev. D **50**, 1173 (1994).

[29] P. Lacock and C. Michael, Phys. Rev. D **52**, 5213 (1995).

[30] D.B. Leinweber and T. Cohen, Phys. Rev. D **49**, 3512 (1994).

[31] M. Göckeler *et al.*, Phys. Rev. D **57**, 5562 (1998).

[32] T. DeGrand (private communication).

[33] F. Bonnet, F. Lee, D. Leinweber, and A. Williams (in progress).